Materials Characterization 174 (2021) 110999

Contents lists available at ScienceDirect

Materials Characterization

journal homepage: www.elsevier.com/locate/matchar

A novel approach to index site-specific grain boundary plane

Xingyu Feng, Jiayu Xie, Wenjun Kuang *

Center for Advancing Materials Performance from the Nanoscale (CAMP-Nano), State Key Laboratory for Mechanical Behavior of Materials, Xi'an Jiaotong University, Xi'an 710049, PR China

ARTICLE INFO

Keywords:
Focused ion beam (FIB)
Electron backscatter diffraction (EBSD)
Transmission Kikuchi diffraction (TKD)
Grain boundary structure

ABSTRACT

A novel approach using focused ion beam (FIB) and electron backscatter diffraction (EBSD) or transmission Kikuchi diffraction (TKD) was developed to characterize all five parameters of the individual grain boundary. With this approach, the grain orientations and the grain boundary trace angles on two perpendicular surfaces can be measured. Then the grain boundary plane normal in the sample coordinate system can be determined and transformed to plane indices in the two crystal coordinate systems. FIB-TKD is a viable alternative to FIB-EBSD when EBSD measurement can't be conducted on the sample surface which is degraded by oxidation or corrosion. This approach was verified on a coherent twin boundary in alloy 690. The accuracy of the present FIB-EBSD method is better than 3°. This approach provides a convenient and efficient solution for measuring all five parameters of a site-specific grain boundary during FIB sample preparation.

1. Introduction

Grain boundary (GB) is a key structure element in polycrystalline material and has critical influence on the performance of the material. Grain boundary engineering [1] has been proposed to improve the overall intergranular properties of material (such as resistance to intergranular stress corrosion cracking) by increasing the proportion of "special boundary" ($\Sigma \leq 29$ coincidence site lattice (CSL) boundary) and optimizing its distribution. The special CSL grain boundary is defined not only by the misorientation between the two neighboring grains, but also by the indices of grain boundary planes. Increasing evidences indicate that not all "special boundaries" defined by grain misorientation show excellent intergranular degradation resistance. Grain boundaries with the same misorientation but different grain boundary plane combinations exhibit different properties, such as coherent and incoherent twin boundaries [2–4]. The correlation between the grain boundary structure and the intergranular property is still not well understood. Recent results show that the index of grain boundary plane, rather than the misorientation, plays a dominant role in grain boundary migration [5–8], intergranular corrosion [9], diffusion [3], adsorption [10, 11], segregation and fracture [12–14]. A concept of grain boundary plane engineering (GBPE) has been proposed to improve the performance of polycrystalline material by maximizing the proportion of grain boundary with low index planes [15]. This concept has attracted increasing attention in recent years as it is considered to be a more effective grain boundary engineering strategy [15–17]. Thus, in order to further establish the linkage between the grain boundary structure and its properties, it is imperative to develop an efficient approach to fully characterize the geometric configuration of grain boundary, especially the grain boundary plane index.

Grain boundary structure can be fully characterized by five geometric degrees of freedom. Three independent parameters are used to describe the relative misorientation between the adjacent grains. The other two describe the orientation of the grain boundary plane. Among the five geometric grain boundary parameters, the misorientation can be directly measured by EBSD. Compared with misorientation, GB plane normal vectors is usually harder to acquire. Several approaches have been tried to determine the index of GB plane. Randle and Dingley first proposed "two surface sectioning methods" to measure the GB plane [18]. Based on this method, Baik et al. [19] investigated the relationship between grain boundary structure and segregation behavior of nickel-base stainless alloy. Recently, a high-throughput technique termed electron diffraction optical reflectance (EDOR) was developed for determining grain boundary character [20]. Similar to the two surface sectioning methods, the EDOR was based on measuring GB misorientation via EBSD and GB plane normal vector via optical reflectance micrograph. The EDOR enables cost- and time-effective assembly of crystallography–property databases for thousands of individual GBs. However, this technique can only be applied on samples with through-thickness grains. EBSD pattern method was also proposed to

* Corresponding author.
E-mail address: wjkuang66@gmail.com (W. Kuang).

https://doi.org/10.1016/j.matchar.2021.110999
Received 1 December 2020; Received in revised form 20 February 2021; Accepted 22 February 2021
Available online 25 February 2021
1044-5803/

characterize the GB plane [21]. It can non-destructively determine grain boundary plane normal inclination angle by comparing simulated grain boundary curve library and experimental curve, with a maximum error of 11°. This technique relies on intensive computer modelling and simulation and can't directly calculate the indices of grain boundary planes. Yu et al. [14] has employed the Kikuchi pattern method and the two-dimensional lattice imaging method to identify the normal of boundary plane. The former method required that the boundary was tilted to edge-on condition with one grain aligned to a known zone axis. Then the grain boundary plane indices can be identified by matching the boundary trace and the parallel Kikuchi bands. If the parallel Kikuchi band doesn't appear, it is necessary to tilting the grain boundary slightly off the edge-on condition. Hence, the error can go up to 8°. Different from EBSD pattern method, the Kikuchi pattern method allows indexing grain boundary planes directly. Hu et al. [11] also indexed grain boundary terminal plane using lattice imaging method with the aid of transmission electron microscope (TEM). Serial sectioning (using focused ion beam (FIB) milling or mechanically polishing) combined with EBSD is usually used to obtain 3D-characterization of grain boundary microstructure, but the method was usually time-consuming and destructive [9, 22–24]. Echlin et al. [25] developed a new femtosecond laser-based technique which allows for a fast serial sectioning, while it was also at the expense of destroying the sample. Wang and Zaefferer [26] applied a pseudo-3D EBSD method to accurately determine grain boundary character, which required a special pre-tilted holder to clamp the sample and can only be used on GBs intersecting the sample edge. Hanson [12] and Bagri [27] have analyzed the grain shape and GB plane orientation in 3 dimensions (3D) by high-energy diffraction microscopy (HEDM). This method requires advanced X-ray sources and significant computation power. It is costly and time-consuming, yet the errors of the boundary plane indexing could be over 10°.

In some cases, investigating the behavior of individual grain boundaries is most beneficial to the study of intergranular behaviors like environmental degradation [28]. Intergranular microstructure analysis based on FIB sample preparation usually needs to be performed on specific grain boundaries which show different behaviors from the rest. It would be desirable to acquire the structures of those site-specific grain boundaries during the FIB sample preparation with readily available resources. In this work, we demonstrate a method for determining the index of GB plane based on FIB-EBSD. To verify the accuracy of this method, a coherent twin boundary was selected for analysis as it can be easily identified and its structure is well understood. A single grain boundary was analyzed twice at two sites with different alignments. This method can be implemented with either EBSD or transmission Kikuchi diffraction (TKD), both of which will be tried here. Subsequently, the source of error during the GB plane indexing is analyzed.

2. Experimental procedure

2.1. Material

The alloy 690 used in this study was solution annealed at 1100 °C for 1 h and water quenched. The average grain size is around 50 μm. The chemical composition (wt%) is 57.6%Ni, 32.7%Cr, 8.64%Fe, 0.25%Mn, 0.315%Al, 0.08%Si and 0.02%C. After being mechanical abraded up to 4000 grit, the coupons were electropolished for 30 s at 30 V in 10% (volume fraction) perchloric acid in methanol at −30 °C and then cleaned immediately with methanol and acetone.

2.2. Microstructural characterization

The grain boundary network on the sample surface was first characterized by SEM. Crystallographic orientation of the sample surface was examined with a Nordlys EBSD detector in a FEI Helios Nanolab 600 systems. After the sample was tilted to 70°, EBSD mapping was obtained at a working distance of 12 mm with a beam voltage of 20 kV and a probe current of 5.5 nA. Prior to FIB milling, two 20 × 1.2 μm rectangular areas across a coherent twin boundary were coated with ~2 μm thick Pt layers. One Pt layer was aligned with the RD direction and the other one was perpendicular to the target GB trace. The cross sections below the Pt layers were trenched out as indicated in Fig. 1. To measure the GB trace angle, a lower accelerating voltage (5 kV) was used to increase spatial resolution and signal-to-noise ratio. Subsequently, the lamellas were lifted-out and attached to a Cu grid, and gradually milled to ~100 nm thick for TKD tests. TKD analysis was performed on the same FIB-EBSD system. The sample was tilted to 18° with respect to the horizontal position, and the working distance was set to 3.5 mm. The Kikuchi patterns were captured at an accelerating voltage of 25 kV and a probe current of 5.5 nA. The step size was set to 20 nm. Then the crystallographic orientation data was post-processed with Channel 5 software.

2.3. Indexing grain boundary planes

In order to acquire the index of GB plane, grain boundary trace angles on two perpendicular sections with respect to the coordinate axis in the sample coordinate system are needed, as shown in Fig. 1. Before the measurement of GB trace angle, the Pt layer direction should be accurately aligned with X axis. Fig. 1(a) shows α angle between the GB trace and X axis on the surface (X-Y plane in the sample coordinate system), and the line trace was designated as vector $A = (\cos\alpha, \sin\alpha, 0)$. It should be mentioned that α denotes the trace angle on the surface where the grain orientations were measured. Likewise, the β angle between GB trace and X axis on X-Z plane was also measured, and the GB trace was designated as vector $B = (\cos\beta, 0, -\sin\beta)$. Therefore, in the sample coordinate system X-Y-Z, the normal of GB plane can be described as:

$$n = \frac{A \times B}{|A \times B|} \tag{1}$$

Orientation of grains which are adjacent to the boundary can be described by Euler angles $<\varphi_1, \Phi, \varphi_2>$. In this paper, the orientation Euler angle is determined by the average grain orientation. To calculate the GB plane indices, the Euler angles need to be converted into an orientation matrices by the following formula:

$$g = \begin{bmatrix} \cos\varphi_1\cos\varphi_2 - \sin\varphi_1\sin\varphi_2\cos\Phi & \sin\varphi_1\cos\varphi_2 + \cos\varphi_1\sin\varphi_2\cos\Phi & \sin\varphi_2\sin\Phi \\ -\cos\varphi_1\sin\varphi_2 - \sin\varphi_1\cos\varphi_2\cos\Phi & -\sin\varphi_1\sin\varphi_2 + \cos\varphi_1\cos\varphi_2\cos\Phi & \cos\varphi_2\sin\Phi \\ \sin\varphi_1\sin\Phi & -\cos\varphi_1\sin\Phi & \cos\Phi \end{bmatrix} \tag{2}$$

Matrix g is used for transformation from the sample coordinate system to the crystal coordinate system. Thus, the index of GB plane normal in two grains can be established by:

$$N1 = g_1 \cdot n \tag{3}$$

$$N2 = g_2 \cdot n \tag{4}$$

Where g_1, g_2 are orientation matrices on both sides of the grain

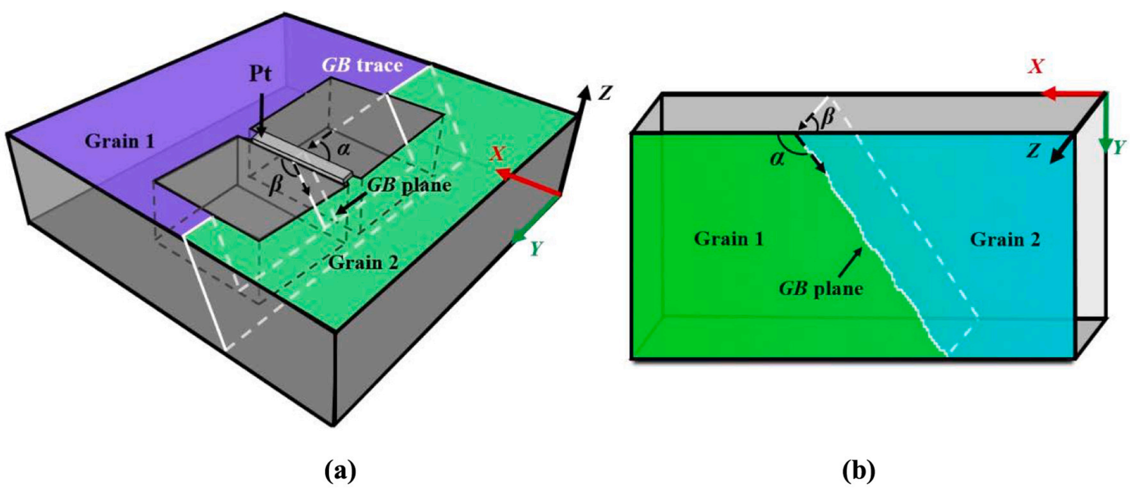

Fig. 1. Schematic showing the trace angle measurement in grain boundary plane indexing by (a) FIB-EBSD method and (b) FIB-TKD method.

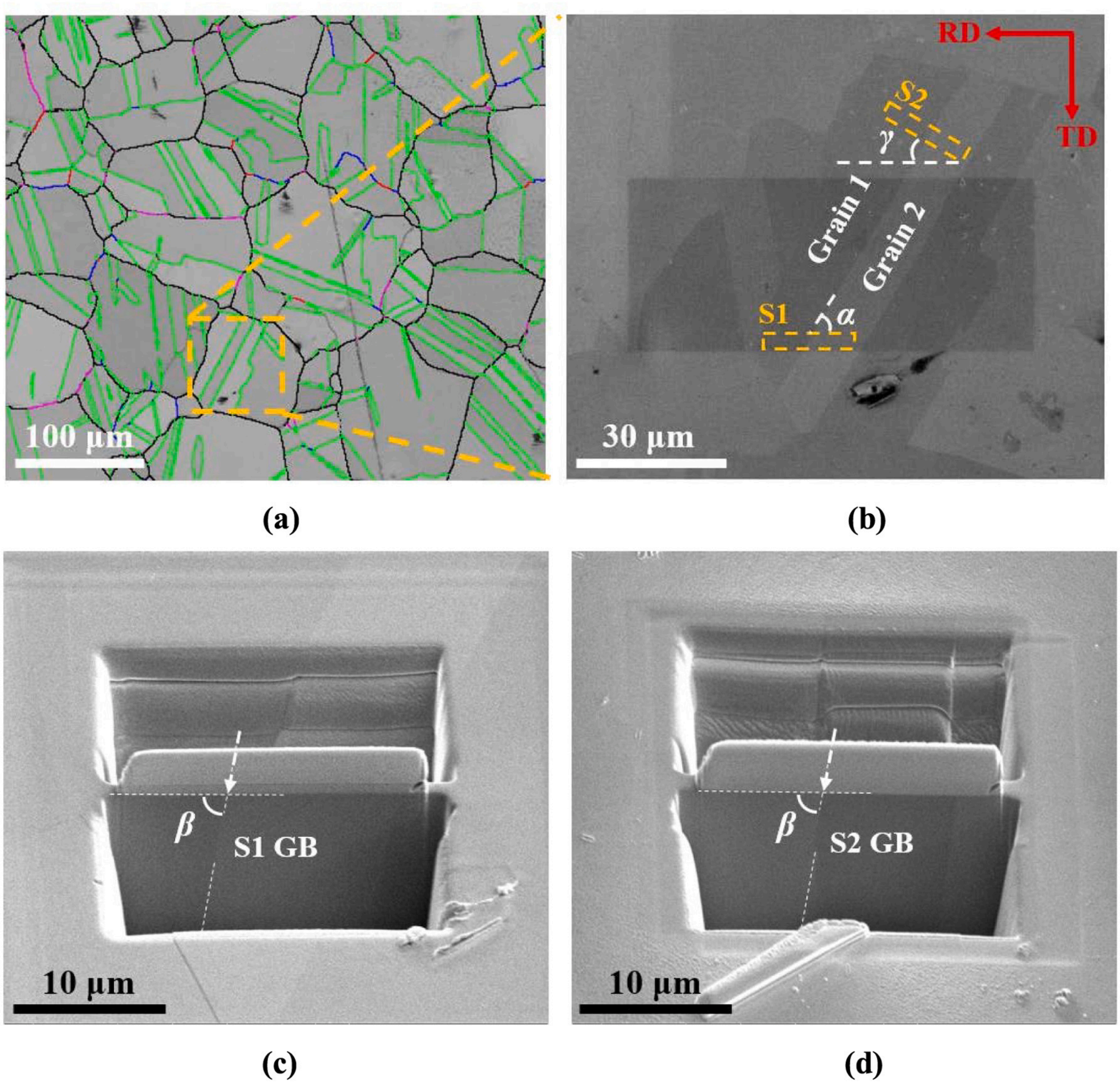

Fig. 2. Identification of the normal of the grain boundary plane by measuring two grain boundary trace angles. (a) Grain boundary mapping; (b) Sample extraction location; (c, d) Cross sections of S1and S2 boundaries processed by FIB.

boundary, and $N1$ and $N2$ represent the normal of GB planes in the two grains, respectively.

It should be noted that if the Pt layer is not aligned with X axis, the orientation matrices of adjacent two grains should be adjusted according to the rotation angle γ around the Z axis:

$$g' = g^* r \tag{5}$$

Where g' is the new matrix after rotation, r is the rotation matrix, it can be expressed as:

$$r = \begin{bmatrix} \cos\gamma & -\sin\gamma & 0 \\ \sin\gamma & \cos\gamma & 0 \\ 0 & 0 & 1 \end{bmatrix} \tag{6}$$

The sign of the rotation angle γ follows the law of the right-hand coordinate system. For the sample where the grain orientations cannot be directly measured by EBSD from the sample surface while the grain boundary trace can be still revealed (such as on oxidized Ni base alloy [29]), the GB plane index can be obtained by the FIB+TKD method using the same principle, as shown in Fig. 1(b). The above calculation can be realized in MATLAB.

3. Results

The grain boundary network is shown in Fig. 2(a). The coherent twin boundaries normally appears as straight parallel lines across the parent grain [2, 30], denoted as green lines in Fig. 2(a). As shown in Fig. 2(b), the Euler angle from the grains on both sides of the S1 boundary were measured. For grain 1 and grain 2, they were (23.73, 35.62, 0.83) and (104.54, 42.04, 77.18) respectively. Accordingly, their orientation matrices can be expressed as:

$$g_1 = \begin{bmatrix} 0.911 & 0.413 & 0.008 \\ -0.340 & 0.738 & 0.582 \\ 0.234 & -0.533 & 0.813 \end{bmatrix}, \; g_2 = \begin{bmatrix} -0.757 & 0.033 & 0.653 \\ 0.085 & -0.985 & 0.149 \\ 0.648 & 0.168 & 0.743 \end{bmatrix}$$

Then the angles between GB traces and X axis on the surface and cross section are measured, $\alpha = 60^\circ$, $\beta = 78.5^\circ$, as shown in Fig. 2(b, c). Thus the vectors of GB line traces are described to be $A = (0.500, 0.866, 0)$, $B = (0.199, 0, -0.980)$ in the sample coordinate system. It should be mentioned that the image needs to be tilt-corrected when measuring β. Subsequently, the normal of GB plane can be determined through eq. (1), which was then converted into the GB plane indices by eqs. (3) and (4). The acquired GB plane indices were labeled as $(-1\ 1\ -1)_{\sim 2.06^\circ}//(1\ -1\ -1)_{\sim 2.10^\circ}$, which means that the actual GB planes are 2.06° and 2.10° off the ideal $(-1\ 1\ -1)$ and $(1\ -1\ -1)$ planes, respectively. If the Pt layer is perpendicular to GB trace which is normally the case during FIB sample cutting, like S2 in Fig. 2(b, d), then $\alpha = 90^\circ$ and $A = (0, 1, 0)$. As mentioned before, the orientation matrices need to be transformed according to rotation angle γ. Here $\gamma = -30^\circ$. According to eqs. (5) and (6), the new orientation matrices of grain 1 and grain 2 are:

$$g_1' = \begin{bmatrix} 0.582 & 0.813 & 0.008 \\ -0.664 & 0.469 & 0.582 \\ 0.470 & -0.345 & 0.813 \end{bmatrix}, \; g_2' = \begin{bmatrix} -0.672 & 0.350 & 0.653 \\ 0.566 & -0.811 & 0.149 \\ 0.477 & 0.470 & 0.743 \end{bmatrix}$$

β was measured to be79.5° as displayed in Fig. 2(d), then the vector $B = (0.182, 0, -0.983)$. Thus, GB plane indices were ultimately calculateded to be $(-1\ 1\ -1)_{\sim 2.57^\circ}//(1\ -1\ -1)_{\sim 2.61^\circ}$.

The FIB-TKD method was also used for indexing the GB planes of the same GB. When the surface of samples cannot meet the EBSD test requirements (such as when the surface was degraded by high temperature oxidation), the orientation of grains cannot be directly obtained. Then TKD can be used to measure the Euler angles of grains. Two FIB lamellas are cut from different sites of the same coherent twin boundary for TKD measurement, named S1-TKD and S2-TKD respectively. Before TKD experiment, the cross section of the sampled CTB on Fig. 2 (d) was analyzed in TEM, as shown in Fig. 3 (a-d). The boundary trace is perpendicular to the normal of the common (111) plane, indicating it is a CTB (Fig. 3 (b-d)). Fig. 3(e) and (f) show the inverse pole figures (IPFs) of S1-TKD and S2-TKD samples. For S1-TKD samples, the Euler angles of the two grains are (324.1, 48.01, 43.54) and (240.23, 12.59, 68.65) respectively and the orientation matrices can be determined according to eq. (2). As the sample drift during TKD measurement can cause distortion of the GB trace, the α angle is measured from the cross section after FIB trenching. The angles between GB traces and X axis on two perpendicular surfaces are $\alpha = 78.5^\circ$ and $\beta = 60^\circ$ (as shown in Fig. 2(b) and (c)) and the corresponding trace vectors $A = (0.1994, 0.980, 0)$ and $B = (0.5, 0, 0.866)$. According to eq (1), the normal of GB plane is described as $n = (0.853, -0.174, -0.492)$ in the sample coordinate system. Then the GB plane indices can be calculated through eqs. (3) and (4), i.e. $(1\ -1\ -1)_{\sim 6.25^\circ}//(1\ 1\ -1)_{\sim 6.36^\circ}$. For S2-TKD sample, the Euler angles from both grains are (78.83, 28.35, 46.48) and (260.9, 41.88, 44.2). Similarly, the GB indices of S2-TKD can also be calculated. The detailed results are summarized in Table 1. Compared to the 3D-EBSD method [9, 25], this technique is more convenient and efficient. It can quickly obtain the GB plane index of any target grain boundary with no need of sophisticated equipment and only induces limited destruction to the sample. Moreover, the acquired accuracy in this work is about 6–8° higher than the previous TEM and HEDM methods [11, 12, 14, 26]. The FIB-TKD method also provides a feasible way to index grain boundary plane when the surface of sample cannot meet the conventional EBSD test requirement.

4. Discussion

The above results indicate that both the methods based on FIB-EBSD and FIB-TKD can effectively measure all the grain boundary parameters. The strategy of the method is to determine the GB plane normal in the sample coordinate system and transform it from the sample coordinate system to the crystal coordinate system. During the indexing process, the errors may result from several factors. Firstly, there is error in the alignment and sample tilting when measuring the grain boundary trace angles (α and β) and collecting Kikuchi diffraction pattern. Secondly, due to the cone-shaped ion beam, the cross section cut by FIB is not perfectly perpendicular to the surface. Those factors would result in errors in the measurements of trace angles and grain orientations and finally influence the accuracy of final achieved GB plane index. However, it is difficult to assess and control the measurement error in the orientation of adjoining grains. Thus, it is more meaningful to analyze the error caused by the measurement of trace angles.

Assuming there is no error in measuring the grain orientations, the deviation of indexed boundary plane was calculated using all the combinations of trace angles near the ideal values. In the case of S1 sample, Fig. 4 shows the evolution of deviation angle from {111} plane with the measured trace angles. From Fig. 4 (a), the deviation angle increases as α angle deviates from 60.3°or β angle deviates from 80.9°. When $\alpha = 60.3^\circ$, $\beta = 80.9^\circ$, the GB plane reaches the ideal {111} plane. Fig. 4 (b) and (c) shows the error changes linearly as a measured trace angle deviates from ideal value when the other one is kept correct. It can be seen from Fig. 4 (a) that the error distribution shows approximately concentric circles around the ideal trace angles. Angle α and angle β measured here are 60° and 78.5° respectively (marked as p in Fig. 4 (a)). It seems that the deviation of angle β from the ideal value causes the majority of error. It should also be noticed that the cone-shaped ion beam of FIB can't guarantee the exposed cross section of the grain boundary is absolutely perpendicular to the sample surface, which will introduce errors into determining the normal of the boundary planes [31, 32]. In general, the cross section trenched out by FIB and sample surface are usually not strictly perpendicular, which is the reason why 1–2° is usually compensated during the thinning process of TEM sample preparation. It also explains why the measured angle β deviates more from the ideal value for S1. The error caused by beam shape can be minimized by reducing beam current during FIB cutting.

Compared with FIB-EBSD, although FIB-TKD allows for better spatial

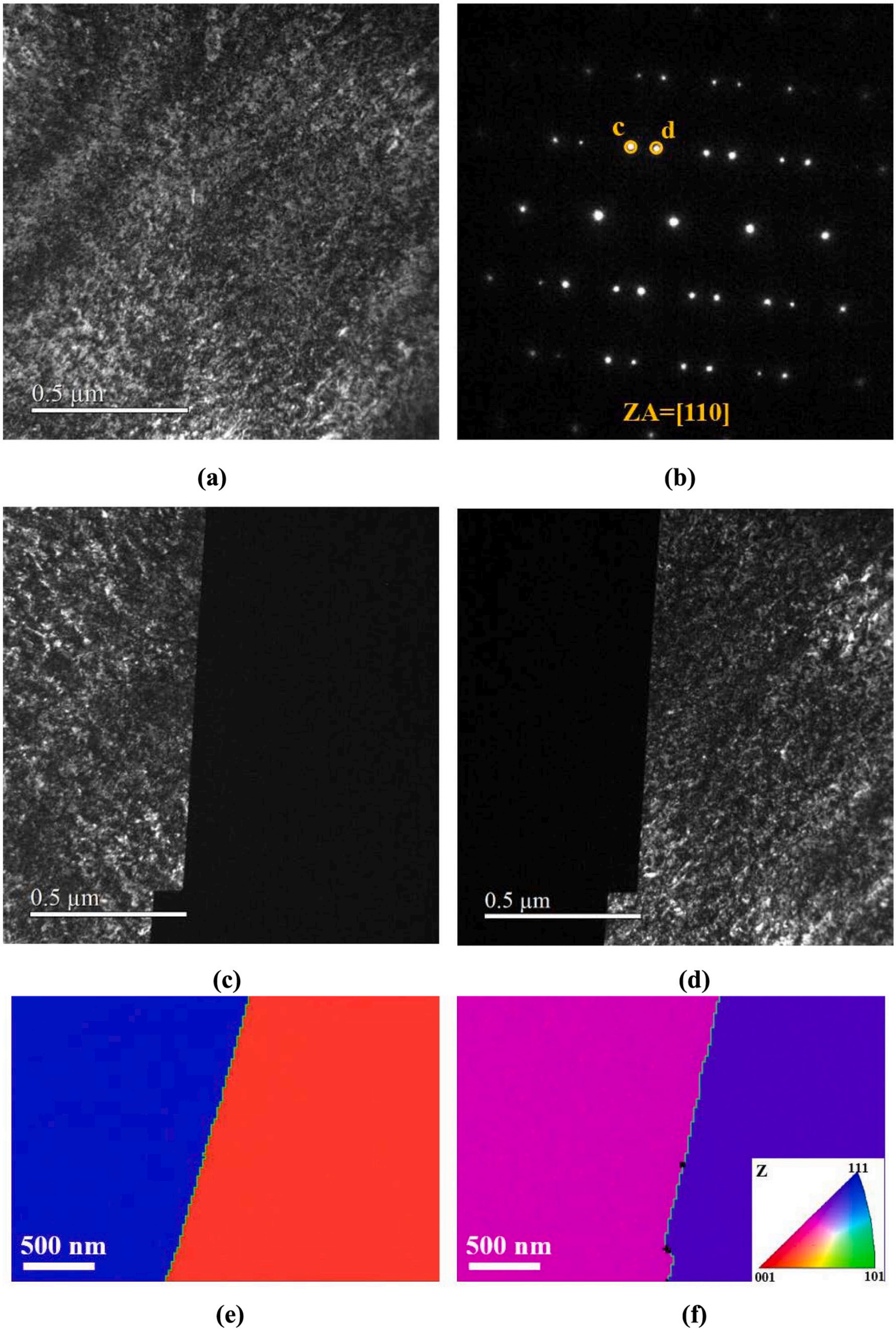

Fig. 3. (a) TEM bright field image and (b) diffraction pattern of the sampled twin boundary; (c, d) dark field images corresponding to spots c and d on (b). (e, f) IPF maps of S1-TKD and S2-TKD samples.

Table 1
Summary of the grain boundary plane index of both adjoining grains from the same coherent twin boundary. The lowest-index best match palane and the deviation between actual planes and ideal planes are given.

GB	α angle (°)	β angle (°)	Grain 1 GB plane normal			Grain 1 Lowest-index best match plane	Grain 1 Deviation (°)	Grain 2 GB plane normal			Grain 2 Lowest-index best match plane	Grain 2 Deviation (°)
S1	60	78.5	−0.575	0.553	−0.603	(−1 1 −1)	2.06	0.548	−0.584	−0.599	(1 −1 −1)	2.10
S2	90	79.5	−0.574	0.547	−0.610	(−1 1 −1)	2.57	0.542	−0.584	−0.605	(1 −1 −1)	2.61
S1-TKD	78.5	60	0.489	−0.621	−0.613	(1 −1 −1)	6.25	0.536	0.525	−0.661	(1 1 −1)	6.36
S2-TKD	79.5	90	−0.624	−0.621	0.475	(−1 −1 1)	6.94	0.530	0.523	−0.667	(1 1 −1)	6.65

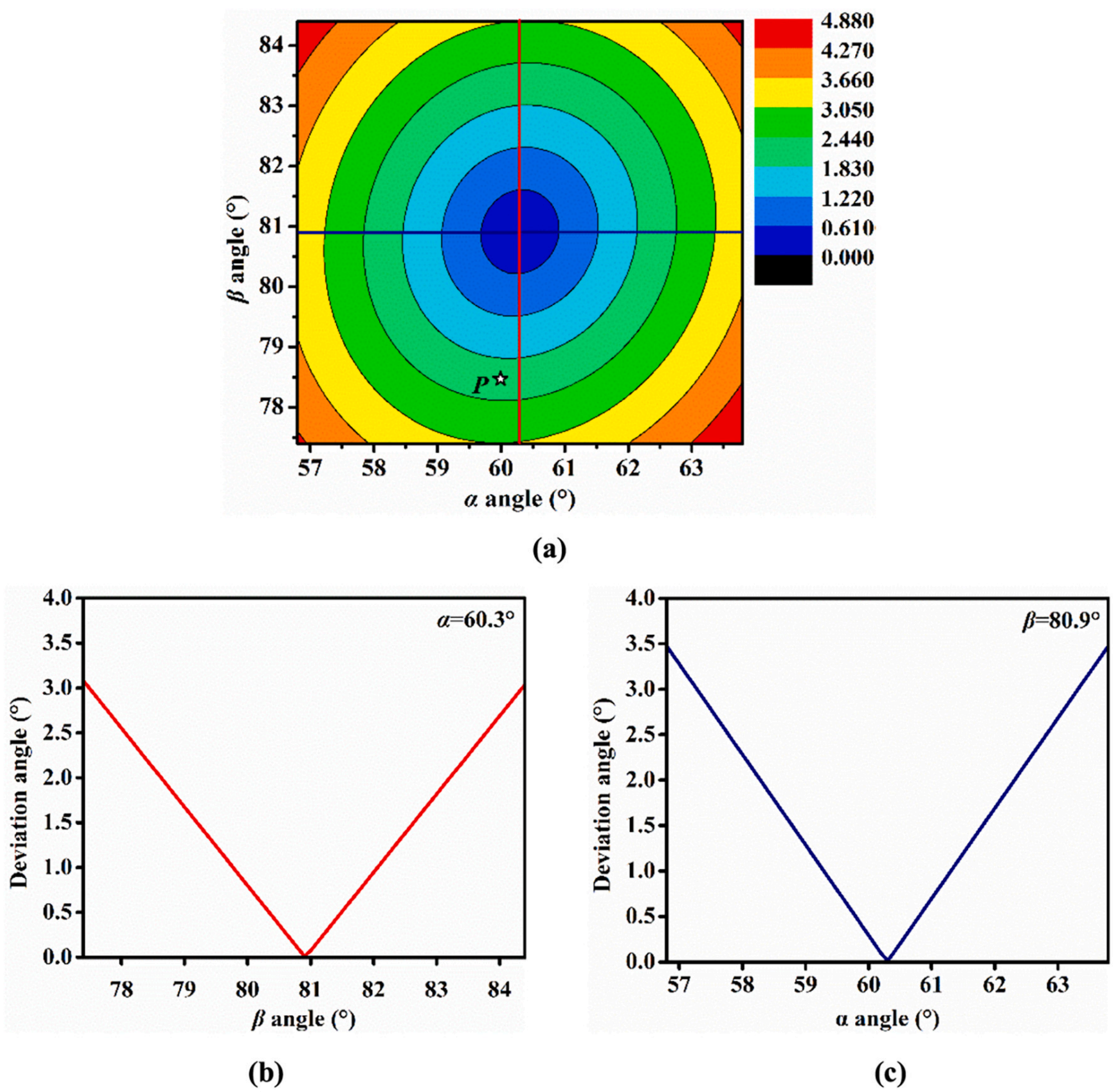

Fig. 4. The evolution of deviation angle with α and β deviating ideal position. (b) and (c) the variation of deviation angle as a function of β angle and α angle along red line and blue line in (a) respectively. (For interpretation of the references to colour in this figure legend, the reader is referred to the web version of this article.)

resolution, the acquired deviation from ideal plane is larger (Table 1). The FIB cross section is probably not cut perfectly perpendicular to the surface during the thinning process which induces error in the calculation of grain boundary plane normal in the sample coordinate system by Eq. (1).

5. Conclusion

In conclusion, the result shows that GB plane index of a site-specific grain boundary can be accurately determined through measuring the grain orientations and the GB trace angles. The grain boundary plane can be accurately indexed within 3°. Therefore, all 5 parameters describing the GB structure can be conveniently and efficiently characterized with the aid of FIB and EBSD. For the sample which precludes the conventional EBSD measurement on the surface, the FIB-TKD technique provides an alternative to index the grain boundary plane. The FIB lamella should be kept perpendicular to the sample surface during FIB cutting. The approach developed in this work could be readily realized during the preparation of FIB sample from a specific grain boundary and the acquired GB parameters could be correlated with other microstructure features (such as intergranular oxide or crack microstructure) from subsequent analysis, facilitating the establishment of structure-performance relationship for grain boundary.

Data availability

The raw/processed data required to reproduce these findings cannot be shared at this time as the data also forms part of an ongoing study.

Declaration of Competing Interest

The authors declare that they have no known competing financial interests or personal relationships that could have appeared to influence the work reported in this paper.

Acknowledgements

We would like to thank Dr. Zijun Ren at Instrument Analysis Center of Xi'an Jiaotong University for his assistance with EBSD analysis. This work was supported by the National Natural Science Foundation of China (No. 51971172) and the Young Talent Support Plan of Xi'an Jiaotong University.

Appendix A. Supplementary data

Supplementary data to this article can be found online at https://doi.org/10.1016/j.matchar.2021.110999.

References

[1] T. Watanabe, An approach to grain boundary design of strong and ductile polycrystals, Res Mechanica 11 (1984) 47–84.
[2] W. Kuang, G.S. Was, The effect of grain boundary structure on the intergranular degradation behavior of solution annealed alloy 690 in high temperature, hydrogenated water, Acta Mater. 182 (2020) 120–130, https://doi.org/10.1016/j.actamat.2019.10.041.
[3] C. Minkwitz, C. Herzig, E. Rabkin, W. Gust, The inclination dependence of gold tracer diffusion along a Σ3 twin grain boundary in copper, Acta Mater. 47 (4) (1999) 1231–1239, https://doi.org/10.1016/S1359-6454(98)00429-7.
[4] H. Miyamoto, K. Ikeuchi, T. Mimaki, The role of grain boundary plane orientation on intergranular corrosion of symmetric and asymmetric [110] tilt grain boundaries in directionally solidified pure copper, Scr. Mater. 50 (12) (2004) 1417–1421, https://doi.org/10.1016/j. scriptamat.2004.03.016.
[5] H.Y. Lee, S.-J.L. Kang, D. Yong, The effect of elastic anisotropy on the direction and faceting of chemically induced grain boundary migration in Al_2O_3, Acta Metall. Mater. 41 (8) (1993) 2497–2502, https://doi.org/10.1016/0956-7151(93)90330-U.
[6] R. Schmelzle, B. Giakupian, T. Muschik, W. Gust, R.A. Fournelle, Diffusion induced grain boundary migration of symmetric and asymmetric ⟨011⟩{011} tilt boundaries during the diffusion of Zn into Cu, Acta Metall. Mater. 40 (5) (1992) 997–1007, https://doi.org/10.1016/0956-7151(92)9007-R.
[7] R. Vook, F. Witt, Thermally induced strains in evaporated films, J. Appl. Phys. 36 (1965) 2169–2171, https://doi.org/10.1063/1.1714442.
[8] F. Witt, R. Vook, Thermally induced strains in cubic metal films, J. Appl. Phys. 39 (1968) 2773–2776, https://doi.org/10.1063/1.1656671.
[9] D. An, T.A. Griffiths, P. Konijnenberg, S. Mandal, Z. Wang, S. Zaefferer, Correlating the five parameter grain boundary character distribution and the intergranular corrosion behaviour of a stainless steel using 3D orientation microscopy based on mechanical polishing serial sectioning, Acta Mater. 156 (2018) 297–309, https://doi.org/10.1016/j.actamat.2018.06.044.
[10] W. Han, M.J. Demkowicz, E. Fu, Y.Q. Wang, A. Misra, Effect of grain boundary character on sink efficiency, Acta Mater. 60 (18) (2012) 6341–6351, https://doi.org/10.1016/j.actamat. 2012.08.009.
[11] T. Hu, S. Yang, N. Zhou, Y. Zhang, J. Luo, Role of disordered bipolar complexions on the sulfur embrittlement of nickel general grain boundaries, Nat. Commun. 9 (1) (2018) 2764, https://doi.org/10.1038/s41467-018-05070-2.
[12] J.P. Hanson, A. Bagri, J. Lind, P. Kenesei, R.M. Suter, S. Gradecak, M. J. Demkowicz, Crystallographic character of grain boundaries resistant to hydrogen-assisted fracture in Ni-base alloy 725, Nat. Commun. 9 (1) (2018) 3386, https://doi.org/10.1038/s41467-018-05549-y.
[13] S. Mandal, K.G. Pradeep, S. Zaefferer, D. Raabe, A novel approach to measure grain boundary segregation in bulk polycrystalline materials in dependence of the boundaries' five rotational degrees of freedom, Scr. Mater. 81 (2014) 16–19, https://doi.org/10.1016/j.scriptamat.2014. 02.016.
[14] Z. Yu, P.R. Cantwell, Q. Gao, D. Yin, Y. Zhang, N. Zhou, G.S. Rohrer, M. Widom, J. Luo, M.P. Harmer, Segregation-induced ordered superstructures at general grain boundaries in a nickel-bismuth alloy, Science 358 (6359) (2017) 97–101, https://doi.org/10.1126/science.aam8256.
[15] V. Randle, 'Special' boundaries and grain boundary plane engineering, Scr. Mater. 54 (6) (2006) 1011–1015, https://doi.org/10.1016/j.scriptamat.2005.11.050.
[16] V. Randle, Role of grain boundary plane in grain boundary engineering, Mater. Sci. Technol. 26 (7) (2010) 774–780, https://doi.org/10.1179/026708309X12567268926641.
[17] V. Randle, R. Jones, Grain boundary plane distributions and single-step versus multiple-step grain boundary engineering, Mater. Sci. Eng. A 524 (1–2) (2009) 134–142, https://doi.org/10.1016/j.msea.2009.06.018.
[18] V. Randle, D.J. Dingley, Measurement of boundary plane inclination in a scanning electron microscope, Scr. Metall. 23 (1989) 1565–1570, https://doi.org/10.1016/0036-9748(89)90129-4.
[19] Baik Sung-Il, M.J. Olszta, S.M. Bruemmer, David N. Seidman, Grain-boundary structure and segregation behavior in a nickel-base stainless alloy, Scr. Mater. 66 (2012) 809–812, https://doi.org/10.1016/j.scriptamat.2012.02.014.
[20] Matteo Seita, Marco Volpi, Srikanth Patala, Ian McCue, Christopher A. Schuh, Maria Vittoria Diamanti, Jonah Erlebacher, Michael J. Demkowicz, A high-throughput technique for determining grain boundary character non-destructively in microstructures with throughthickness grains, npj Comput. Mater. 2 (2016) 16016, https://doi.org/10.1038/npjcompumats.2016.16.
[21] C. Sorensen, J.A. Basinger, M.M. Nowell, D.T. Fullwood, Five-parameter grain boundary inclination recovery with EBSD and interaction volume models, Metall. Mater. Trans. A 45 (2014) 4165–4172, https://doi.org/10.1007/s11661-014-2345-7.
[22] V. Randle, Application of EBSD to the analysis of interface planes: evolution over the last two decades, J. Microsc. 230 (2008) 406–413, https://doi.org/10.1111/j.1365-2818.2008.02000.x.
[23] T. Liu, S. Xia, T. Shoji, Q. Bai, B. Zhou, Y. Lu, The topology of three-dimensional grain boundary network and its influence on stress corrosion crack propagation characteristics in austenitic stainless steel in a simulated BWR environment, Corros. Sci. 129 (2017) 161–168, https://doi.org/10.1016/j.corsci.2017.10.003.
[24] T. Liu, S. Xia, B. Zhou, Q. Bai, G.S. Rohrer, Three-dimensional characteristics of the grain boundary networks of conventional and grain boundary engineered 316L stainless steel, Mater. Charact. 133 (2017) 60–69, https://doi.org/10.1016/j.matchar.2017.09.026.
[25] M.P. Echlin, N.S. Husseini, J.A. Nees, T.M. Pollock, A new femtosecond laser-based tomography technique for multiphase materials, Adv. Mater. 23 (2011) 2339–2342, https://doi.org/10.1002/adma.201003600.
[26] Z. Wang, S. Zaefferer, On the accuracy of grain boundary character determination by pseudo-3D EBSD, Mater. Charact. 130 (2017) 33–38, https://doi.org/10.1016/j.matchar.2017.05.023.
[27] A. Bagri, J.P. Hanson, J. Lind, P. Kenesei, R.M. Suter, S. Gradecak, M. J. Demkowicz, Measuring grain boundary character distributions in Ni-base alloy 725 using high-energy diffraction microscopy, Metall. Mater. Trans. A 48 (1) (2017) 354–361, https://doi.org/10.1007/s11661-016-3831-x.
[28] A. King, G. Johnson, D. Engelberg, W. Ludwig, J. Marrow, Observations of intergranular stress corrosion cracking in a grain-mapped polycrystal, Science 321 (2008) 382–385, https://doi.org/10.1126/science.1156211.
[29] Wenjun Kuang, Gary S. Was, A high-resolution characterization of the initiation of stress corrosion crack in alloy 690 in simulated pressurized water reactor primary water 163 (2020) 108243, https://doi.org/10.1016/j.corsci.2019.108243.
[30] W. Kuang, G.S. Was, C. Miller, M. Kaufman, T. Alam, B. Gwalani, R. Banerjee, The effect of cold rolling on grain boundary structure and stress corrosion cracking susceptibility of twins in alloy 690 in simulated PWR primary water environment, Corros. Sci. 130 (2018) 126–137, https://doi.org/10.1016/j.corsci.2017.11.002.
[31] A. Lugstein, B. Basnar, G. Hobler, E. Bertagnolli, Current density profile extraction of focused ion beams based on atomic force microscopy contour profiling of nanodots, J. Appl. Phys. 92 (7) (2002) 4037–4042, https://doi.org/10.1063/1.1505685.
[32] R. Nassar, M. Vasile, W. Zhang, Mathematical modeling of focused ion beam microfabrication, J. Vac. Sci. Technol. B 16 (1) (1998) 109–115, https://doi.org/10.1116/1.589763.